All-optical switching in 2D silicon photonic crystals with low loss waveguides and optical cavities

Michele Belotti, Juan F. Galisteo-López[†], Sara De Angelis, Matteo Galli, Ivan Maksymov[*] and Lucio Claudio Andreani

Dipartimento di Fisica "A. Volta" and UdR CNISM
Università degli Studi di Pavia, via Bassi 6, 27100 Pavia, Italy
[†]*present address: Instituto de Ciencia de Materiales de Madrid (CSIC)*
C/Sor Juana Ins de la Cruz 3, 28049 Madrid, Spain
[*]*present address: Microwave and Optoelectronics Laboratory,*
Faculty of Electronic Engineering,
Kharkov National University of Radio Electronics,
14, Lenin Ave. 61166 Kharkov, Ukraine

David Peyrade

LTM, CNRS, 17 rue de Martyrs, F-38054 Grenoble, France

Yong Chen

École Normale Supérieure, Département de Chimie,
24 rue Lhomond , 75231 Paris Cedex 05 France
LPN-CNRS, route de Nozay, F-91460 Marcoussis, France
belotti@fisicavolta.unipv.it

Abstract: A study of the optical transmission of low-loss W1.5 photonic crystal waveguides built on silicon membranes and operating at telecom wavelengths is presented. The feasibility of performing all-optical switching is demonstrated for W1.5 waveguides coupled with L3 cavities, systems amenable for incorporation in on-chip devices. Switching of waveguide transmission is achieved by means of optical excitation of free carriers using a 2.5 ns pump laser. Experimental results are reproduced by finite-difference time-domain simulations which model the response of the finite system and band structure calculations describing the infinite, ideal one.

OCIS codes: (130.4815) Optical switching devices; (130.5296) Photonic crystal waveguides.

References and links

1. J. Joannopoulos, R. Meade, and J. Winn, *Photonic Crystals: Molding the Flow of Light* (Princeton University Press, 1995).
2. K. Sakoda, *Optical Properties Of Photonic Crystals* (Springer, 2005).
3. Y. Vlasov, M. O'Boyle, H. Hamann, and S. McNab, "Active control of slow light on a chip with photonic crystal waveguides." Nature (London) **438**, 65 (2005).
4. I. Märki, M. Salt, H. Herzig, R. Stanley, L. El Melhaoui, P. Lyan, and J. Fedeli, "Optically tunable microcavity in a planar photonic crystal silicon waveguide buried in oxide," Opt. Lett. **31**, 513 (2006).
5. Q. Xu, B. Schmidt, S. Pradhan, and M. Lipson, "Micrometre-scale silicon electro-optic modulator." Nature (London) **435**, 325 (2005).
6. B. Schmidt, Q. Xu, J. Shakya, S. Manipatruni, and M. Lipson, "Compact electro-optic modulator on silicon-on-insulator substrates using cavities with ultra-small modal volumes," Opt. Express **15**, 3140 (2007).

#95023 - $15.00 USD Received 15 Apr 2008; revised 14 Jul 2008; accepted 14 Jul 2008; published 18 Jul 2008

7. K. ichi Umemori, Y. Kanamori, and K. Hane, "Photonic crystal waveguide switch with a microelectromechanical actuator," Appl. Phys. Lett. **89**, 021102 (2006).
8. S. Leonard, H. van Driel, J. Schilling, and R. Wehrspohn, "Ultrafast band-edge tuning of a two-dimensional silicon photonic crystal via free-carrier injection," Phys. Rev. B **66**, 161102 (2002).
9. H. W. Tan, H. M. van Driel, S. L. Schweizer, R. B. Wehrspohn, and U. Gösele, "Nonlinear optical tuning of a two-dimensional silicon photonic crystal," Phys. Rev. B (Condensed Matter and Materials Physics) **70**, 205110 (2004).
10. V. Almeida, C. Barrios, R. Panepucci, and M. Lipson, "All-optical control of light on a silicon chip," Nature (London) **431**, 1081 (2004).
11. V. Almeida, C. Barrios, R. Panepucci, M. Lipson, M. Foster, D. Ouzounov, and A. Gaeta, "All-optical switching on a silicon chip," Opt. Lett. **29**, 2867 (2004).
12. M. Notomi, A. Shinya, S. Mitsugi, G. Kira, E. Kuramochi, and T. Tanabe, "Optical bistable switching action of Si high-Q photonic-crystal nanocavities," Opt. Express **13**, 2678 (2005).
13. F. Ndi, J. Toulouse, T. Hodson, and D. Prather, "All-optical switching in silicon photonic crystal waveguides by use of the plasma dispersion effect," Opt. Lett. **30**, 2254 (2005).
14. T. Tanabe, M. Notomi, S. Mitsugi, A. Shinya, and E. Kuramochi, "All-optical switches on a silicon chip realized using photonic crystal nanocavities," Appl. Phys. Lett. **87**, 151112 (2005).
15. T. Tanabe, K. Nishiguchi, A. Shinya, E. Kuramochi, H. Inokawa, M. Notomi, K. Yamada, T. Tsuchizawa, T. Watanabe, H. Fukuda, H. Shinojima, and S. Itabashi, "Fast all-optical switching using ion-implanted silicon photonic crystal nanocavities," Appl. Phys. Lett. **90**, 031115 (2007).
16. X. Yang, C. Husko, C. W. Wong, M. Yu, and D.-L. Kwong, "Observation of femtojoule optical bistability involving Fano resonances in high-Q/V[sub m] silicon photonic crystal nanocavities," Appl. Phys. Lett. **91**, 051113 (2007).
17. M. Först, J. Niehusmann, T. Plötzing, J. Bolten, T. Wahlbrink, C. Moormann, and H. Kurz, "High-speed all-optical switching in ion-implanted silicon-on-insulator microring resonators," Opt. Lett. **32**, 2046 (2007).
18. D. Gerace and L. Andreani, "Low-loss guided modes in photonic crystal waveguides," Opt. Express **13**, 4939 (2005).
19. M. Galli, D. Bajoni, M. Patrini, G. Guizzetti, D. Gerace, L. Andreani, M. Belotti, and Y. Chen, "Single-mode versus multimode behavior in silicon photonic crystal waveguides measured by attenuated total reflectance," Phys. Rev. B **72**, 125322 (2005).
20. P. Velha, E. Picard, T. Charvolin, E. Hadji, J. Rodier, P. Lalanne, and D. Peyrade, "Ultra-High Q/V Fabry-Perot microcavity on SOI substrate," Opt. Express **15**, 16090 (2007).
21. L. C. Andreani and D. Gerace, "Photonic-crystal slabs with a triangular lattice of triangular holes investigated using a guided-mode expansion method," Phys. Rev. B (Condensed Matter and Materials Physics) **73**, 235114 (2006).
22. A. Taflove and S. Hagness, *Computational electrodynamics: the finite-difference time-domain method* (Artech House, 2005).
23. J. Roden and S. Gedney, "Convolutional PML (CPML): An efficient FDTD implementation of the CFS-PML for arbitrary media," Microw. Opt. Tech. Letters **27**, 334 (2000).
24. Y. Akahane, T. Asano, B. Song, and S. Noda, "High-Q photonic nanocavity in a two-dimensional photonic crystal," Nature (London) **425**, 944 (2003).
25. K. Sokolowski-Tinten and D. von der Linde, "Generation of dense electron-hole plasmas in silicon," Phys. Rev. B **61**, 2643 (2000).
26. T. G. Euser and W. L. Vos, "Spatial homogeneity of optically switched semiconductor photonic crystals and of bulk semiconductors," J. Appl. Phys. **97**, 043102 (2005).
27. E. Palik, *Handbook of Optical Constants of Solids, Vol. 1* (Academic Press, 2004).
28. S. McNab, N. Moll, and Y. Vlasov, "Ultra-low loss photonic integrated circuit with membrane-type photonic crystal waveguides," Opt. Express **11**, 2927 (2003).

1. Introduction

Periodically structuring a dielectric material in the sub-micrometer range can strongly modify its dispersion relation for optical wavelengths, allowing the control of light propagation and emission in ways not conceivable with its unstructured counterpart. Such periodic dielectrics, commonly termed photonic crystals (PhC) [1, 2], have brought a great interest in both fundamental research and advanced applications. For example, high resolution spatial light confinement which is usually difficult to achieve with conventional material processing can be obtained by judiciously tailoring the dispersion properties with advanced nanofabrication techniques. Consequently, light-matter interaction can be greatly enhanced, allowing development

#95023 - $15.00 USD Received 15 Apr 2008; revised 14 Jul 2008; accepted 14 Jul 2008; published 18 Jul 2008

of a number of new devices.

Although a large number of work has already been done to demonstrate the fabrication feasibility of PhCs in different dimensionalities and with different materials, silicon based two dimensional (2D) PhCs have particular interest for future integrated photonic circuits. The choice for such systems has been based mainly by two facts. On the one hand, the high refractive index of silicon makes it an ideal component for the creation of photonic structures with strong light confinement. On the other hand, the fabrication of silicon-based photonic devices has benefited from some of the well established processes of the microelectronic industry that gives the possibility to fabricate high quality PhC samples. Furthermore using silicon raises the possibility to integrate photonic circuits with microelectronic components.

In designing an all-optical integrated circuit (IC), certain components are indispensable such as waveguides (WG), routers, wavelength demultiplexing (WDM) devices, but after all, switches will lay at the heart of logic processing. By using photonic crystals, it should be possible to modify the optical response of the system in a fast time scale. Although certain proposals have been presented and demonstrated based on non optical methods (such as thermo-optic [3, 4], electro-optic [5, 6] or mechanical processes [7]), it is acknowledged that all optical switching is the best route to achieve fast response times for signal processing. In this direction, a number of works have been recently published where resonant and non resonant optical processes [4, 8–17] have been employed as the switching mechanism, successfully showing the feasibility of performing optical switching with low energy consumption.

In the present work we demonstrate all-optical switching in systems amenable for implementation in all optical IC. In particular, we employ 2D PhC fabricated in silicon membranes containing increased channel width waveguides [18, 19], isolated or coupled to optical nanocavities, and compare with previous work on PhC waveguides [12]. Since propagation losses decrease on increasing the channel width, the present configuration can be interesting for switching applications in structures with lower losses. After an initial characterization of the optical response of the system by means of linear waveguide transmission, all-optical switching employing a cavity mode is achieved with low powers using free-carrier generation as the physical mechanism to modify the optical properties of the PhC. The switching time is limited by the nanosecond laser pulse and not by the recombination process in the Si backbone, which can be notably faster [12]. By appropriately tuning the probe beam with respect to the studied cavity mode we are able to simulate ON/OFF and OFF/ON scenarios introducing negligible absorption for the probe beam. Experimental results are successfully reproduced by means of photonic band structure calculations and finite-difference time-domain (FDTD) numerical simulations.

2. Experiment

2.1. Sample preparation

The samples employed in the present work were fabricated using standard electron beam lithography and reactive ion etching techniques on silicon-on-insulator (SOI) wafers (SOITEC™) having a 200 nm silicon core layer and a 1000 nm SiO_2 layer [20]. They consist of free-standing silicon membranes patterned with a triangular lattice of air holes (lattice parameter $a = 420$ nm, hole radius $r/a = 0.32$) containing W1.5 waveguides, both isolated and coupled to L3 cavities. W1.5 waveguides are obtained by creating a line defect along the ΓK direction of the triangular lattice, having a width $w = 1.5 \cdot \sqrt{3}a = 1.5w_0$ along the ΓM direction, where $w_0 = \sqrt{3}a$ is the channel width of a normal W1 waveguide. Such waveguides are known to be best suited for a membrane configuration in terms of light guiding in monomode operation with high group velocity and robustness against extrinsic losses [18, 19].

The L3 cavities, that consist of three missing holes in the waveguide, are placed inside the

#95023 - $15.00 USD Received 15 Apr 2008; revised 14 Jul 2008; accepted 14 Jul 2008; published 18 Jul 2008

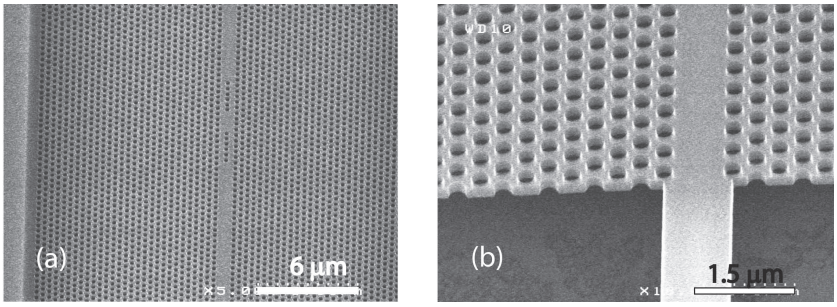

Fig. 1. Scanning electron microscopy images of the samples showing (a) a top view of the cavity region and (b) a detail of the access ridge waveguide.

W1.5 waveguides by introducing two sets of holes which act as Bragg reflectors. The cavity quality factor Q was optimized employing numerical calculations (see below) to evaluate the effect of the number, position and diameter of the holes comprising the Bragg reflector. Access to the PhC area (20 μm and 500 μm wide in the direction perpendicular and parallel to the W1.5 waveguide respectively) for optical probing is achieved by means of access ridge waveguides of length between 300 and 400 μm. These access waveguides have a width of 500 nm and are designed to operate in a monomode regime at the probe wavelength. Their width is gradually increased as the sample entrance is approached in order to minimize coupling losses at the waveguide-PhC interface by matching the channel width of the W1.5 waveguide. Figure 1 shows scanning electron microscopy (SEM) images of typical samples.

2.2. Optical characterization

Linear transmission was measured with a continuous wave (CW) laser tuneable between 1350 and 1630 nm (SANTEC 210-F) delivered onto the optical set-up by a single–monomode polarization maintaining fibre. The incident probe beam is polarized along the plane of the periodicity (i.e. TE polarized). It is focussed to and collected from the access ridge WGs by a pair of high numerical aperture objectives. The transmitted beam is then spatially filtered by a 2 μm core fibre and a Glan-Taylor polarizer to remove spurious substrate-guided light. Collection of transmitted light is performed with an InGaAs detector connected to a lock-in amplifier. Figure 2 shows a schematic diagram of the experimental set-up.

Three observation lines were added to the experimental set-up in order to image the entrance and exit WGs as well as the top surface of the PhC sample with an IR camera (not shown in the figure). This helped during the alignment procedure and provided a qualitative estimate of optical losses (due to coupling and disorder induced scattering) and transmission.

For the switching experiments, optical pumping is performed with a Q-switched Nd:YAG laser with a pulse width of 2.5 ns and a repetition rate of 11 kHz (Impex High-Tech). The pump beam is frequency doubled with a KTP crystal and launched normally to the sample surface employing one of the observation lines. The pump beam is focussed to a 4 μm radius spot which contains only a small sample region around the optical cavity. Finally, the transmitted probe signal collected by the InGaAs detector when pumping the sample is amplified with a voltage amplifier (200 kHz - 2 GHz bandwidth) and registered by an oscilloscope operating with a 1 GHz bandwidth and 4 GHz sampling rate (Agilent). Part of the original pump beam is diverted from the pump line and used to trigger the oscilloscope.

#95023 - $15.00 USD Received 15 Apr 2008; revised 14 Jul 2008; accepted 14 Jul 2008; published 18 Jul 2008

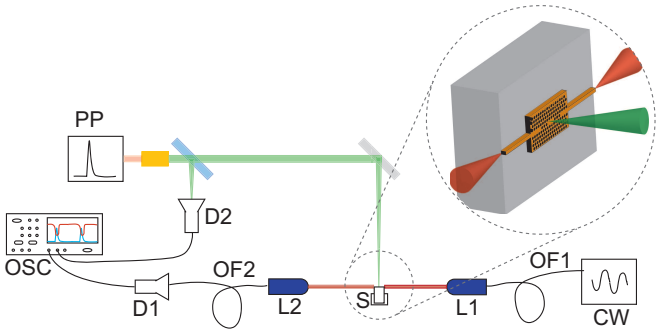

Fig. 2. (Color online) Schematic view of the set-up. The probe beam coming from a CW laser is focussed on the sample (S) and collected by high numerical aperture objectives (L1, L2) and optical fibres (OF1, OF2). The transmitted probe beam is collected by an InGaAs detector (D1) connected to an oscilloscope (OSC). An additional line delivers a pulsed pump beam (PP) into the sample surface in order to locally modify its refractive index. Part of the pump beam is collected with a photodiode (D2) and used as trigger.

3. Theory

3.1. Photonic band structure calculations

For all calculations we have assumed a refractive index of $n_0 = 3.479$ for Silicon in the absence of optical pumping. Calculations of photonic mode dispersion in the W1.5 waveguides and design of cavity structures were performed by means of a guided-mode expansion (GME) method, which consists of expanding the magnetic field on the basis of guided modes of an effective homogeneous waveguide and calculating out-of-plane diffraction losses by perturbation theory [21]. For the self-standing membrane, taking the z axis to be perpendicular to the slab we exploit specular reflection $\hat{\sigma}_{xy}$ with respect to a mirror plane bisecting the slab and calculate only even (TE-like) modes. Furthermore, for W1.5 waveguides and cavity structures, we take advantage of specular reflection symmetry $\hat{\sigma}_{kz}$ with respect to a mirror plane bisecting the channel and distinguish the modes according to $\sigma_{kz} = +1$ (even) or $\sigma_{kz} = -1$ (odd). Notice that for TE-like modes with $\sigma_{kz} = -1$, the dominant electric-field component is spatially even across the channel. Previous calculations have shown that the W1.5 waveguide supports a defect mode below the light line with high group velocity and ultra low losses [18, 19].

3.2. FDTD

Calculations of transmission spectra and spatial distributions of the electromagnetic field in samples containing L3 cavities within the W1.5 waveguide were performed by means of a 3D FDTD method, which consists of solving the Maxwell's equations in space and time without mathematical approximations [22]. The leapfrogging in time followed by implementation of staggered spatial grids leads to an accurate evaluation of the relevant derivatives via finite differences. Absorption of the field components approaching the boundaries of the spatial grids is guaranteed by implementation of the CPML absorbing boundary conditions [23]. A bandpass Gaussian pulse with a half-width t_w=12.8 fs and a time delay $t_0 = 3t_w$ is employed at $t = 0$ as the initial condition. The numerical simulation of the propagation of this pulse reproduces the conditions of the full-scale study, i.e. a single run of the FDTD program results in time-domain data containing information about the propagation of the electromagnetic field at wavelengths between 1350 and 1630 nm. Transmission spectra are next obtained from these time-domain data using a high-resolution Fourier transform. Spatial distributions of the electromagnetic field

#95023 - $15.00 USD Received 15 Apr 2008; revised 14 Jul 2008; accepted 14 Jul 2008; published 18 Jul 2008

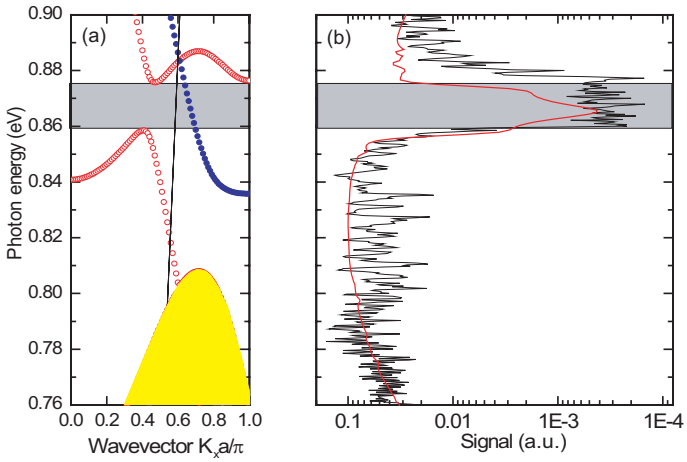

Fig. 3. (Color online) (a) Band structure of a 2D PhC containing a W1.5 line defect. Globally odd (even) defect modes appear as open-red (filled-blue) circles. Filled yellow region indicates bulk PhC modes. Grey band corresponds to a miniband of forbidden frequencies. (b) Experimental and calculated (FDTD) transmission spectra appear as black and red lines respectively.

are obtained simultaneously by performing a running Fourier transform at every gridpoint of the computation domain for each frequency of interest.

In order to obtain exact results and keep within available computer resources, the access ridge waveguides of the FDTD model were shortened to 1.5 μm and each unit cell of the 2D PhC was comprised by $24 \times 24 \times 11$ meshes of the spatial grid having dimensions $\Delta x = \Delta y = 17.5$ nm and $\Delta z = 17.455$ nm. The time-step $\Delta t = 0.3199$ fs was taken equal to the Courant stability limit multiplied by 0.95. The W1.5 waveguide was 20 lattice periods long and the lateral mirrors were 6 periods wide.

The GME and FDTD methods were also used to optimize the quality factor Q of the L3 cavity. A number of calculations were performed to evaluate the effect of the number, position and radii of the holes comprising the Bragg reflectors. At first, transmission spectra of the cavities comprised by the Bragg reflectors with 3, 4, 5, 6 and 7 holes were studied. The structures that possessed minimal losses and maximal Q were then further improved in order to optimize the confinement of the electromagnetic field within the cavity [24]. The radii of the extreme holes of the Bragg reflectors were decreased and their position was shifted. The best field confinement was obtained for the case of 6 air holes in each Bragg reflectors with the nearby holes shifted outwards by $0.18a$ and with their radius being reduced by $0.06a$.

4. Results and discussion

4.1. Linear Transmission

Figure 3 shows the measured transmission spectrum of a W1.5 sample together with a numerical simulation obtained with FDTD. The spectra are compared with the dispersion relation of the infinite crystal. The band structure shows both even and odd TE-like modes, the latter being the relevant ones for our experimental configuration as mentioned in Section 3.

The fundamental TE mode of the access ridge WG is globally odd (the dominant electric field component is spatially even), and can therefore couple to odd modes of the PhC membrane. Accordingly, in the experiment we observe a strong dip in transmission taking place between

#95023 - $15.00 USD Received 15 Apr 2008; revised 14 Jul 2008; accepted 14 Jul 2008; published 18 Jul 2008

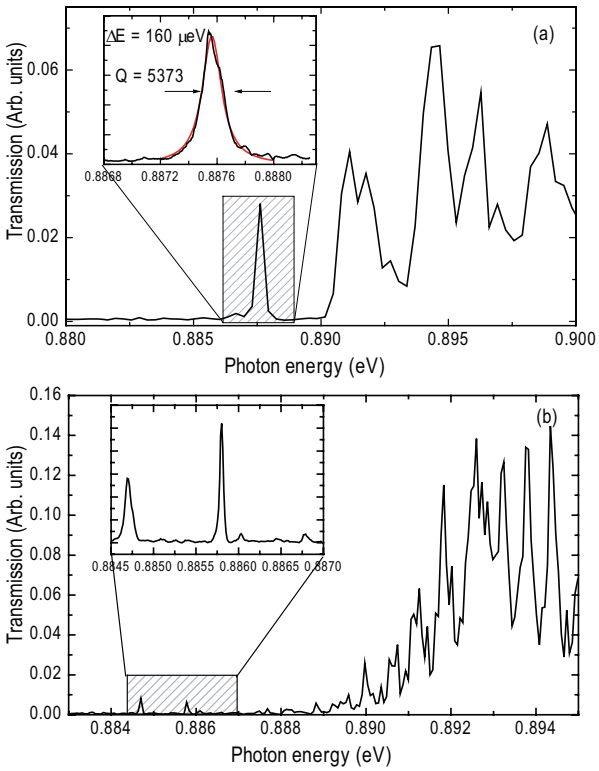

Fig. 4. (Color online) Transmission spectra for two different samples containing L3 cavities within W1.5 waveguides, created by introducing two sets of Bragg mirrors containing 6 (a) and 5 (b) holes. Insets show high resolution spectra of the selected region. Red line in (a) is a Lorentzian fit.

0.86 and 0.875 eV, corresponding to the mini-stop band which appears in the dispersion relation for odd modes. For those frequencies contained within the mini-stop band, the transmitted intensity is attenuated by nearly three orders of magnitude with respect to the transmission in the spectral regions where guided modes are available. Besides the existence of a dip, we see that the transmission spectrum presents strong secondary oscillations. These are Fabry-Perot fringes related to the fact that the overall sample presents three distinct regions, the two access waveguides and the PhC W1.5, with strong reflections at their interfaces as a consequence of impedance mismatch, and different effective refractive indices. Nevertheless, the presence of these finite size effects does not hinder the observation of the transmission dip and we are then able to experimentally identify the presence of the stop band, whose position coincides well with the theoretical prediction.

Together with the experimental spectrum we have plotted the one obtained with the FDTD method. In the numerical simulation, identical parameters to those employed in the band structure calculation were used, i.e. lattice parameter $a = 420$ nm, hole radius $r/a = 0.32$. The modeled structure was designed to have much shorter access waveguides to the sample region than in the experimental case (1.5 and 400 micron respectively). As a consequence, Fabry-Perot oscillations are not observed in the numerical calculations. We can see that the FDTD simulation also presents a strong dip in the spectral range where the band structure predicts the presence of the stop band. This fact indicates that despite the finiteness of the sample, its optical behavior is well reproduced by energy bands calculated for the infinite system. Thus the two calculations

#95023 - $15.00 USD Received 15 Apr 2008; revised 14 Jul 2008; accepted 14 Jul 2008; published 18 Jul 2008

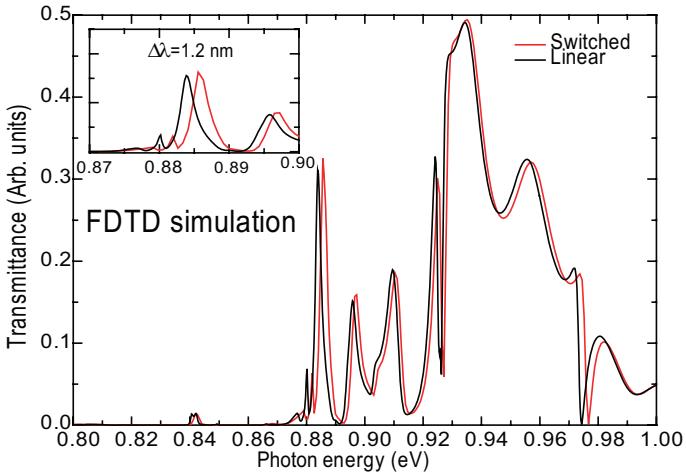

Fig. 5. (Color online) Transmission spectra for a sample containing an L3 cavity within a W1.5 waveguide, created by introducing two sets of Bragg mirrors containing 6 holes. The black curve shows the FDTD linear spectrum calculated using the bulk silicon refractive index n_0 and the red one the switched FDTD simulation obtained by locally changing the refractive index of the cavity to $n = 3471$ (see text). Inset shows a zoomed image of the lowest energy transmission peak.

and the experiment agree well with each other. Finally, we must note some small discrepancies between calculated and measured transmission spectra regarding the attenuation and spectral width of the dip. These are likely caused by the presence of structural imperfections in the fabricated sample, not taken into account in the numerical simulation, that generate extinction whose effect becomes more noticeable with increasing frequency.

We next consider the linear transmission of samples containing L3 cavities within the W1.5 waveguides. Figure 4(a) and 4(b) show transmission spectra for two different samples for which the L3 cavities were created introducing two sets of Bragg mirrors of 6 and 5 holes respectively (samples A and B in what follows). In both cases, the overall behavior is quite similar. Transmission abruptly drops for frequencies below 0.89 eV, coinciding with the high energy edge of the photonic band gap for $\sigma_{xy} = +1$ or TE-like polarization in the bulk crystal. Close to the band edge, some sharp resonances appear, whose spectral position and quality factor vary depending on the sample. For sample A (see Fig. 4(a)), one single peak is observed, located at an energy of 0.8875 eV and having Q=5373, extracted from a high resolution spectrum shown in the inset of the figure. For sample B two peaks are observed, located at 0.8858 and 0.8846 eV, having Q-factors of 8267 and 12475 respectively (see Fig. 4(b)). Besides the difference in spectral positions and Q, we can see that the peaks in sample B transmit only a small fraction (about 7%) of the transmission intensity at the band region. This fact renders the sample less convenient for switching experiments as the transmitted signal is too small to be clearly discriminated from noise. Hence, in what follows we concentrate on sample A.

The linear transmission of sample A was reproduced with FDTD numerical simulations. Figure 5 (black line) shows a calculated spectrum where we can see how the main features of the experimental result, regarding the existence of a band edge near 0.92 eV and some isolated transmission peaks for smaller energies, are well reproduced. Albeit with a different Q, a transmission peak appears for a similar frequency to the one observed in the experiment (0.885 eV).

We have also modeled the behavior of the system under the optical pump beam by locally lowering the refractive index of a circular zone centered on the cavity by 0.2% (from $n_0 = 3.479$

#95023 - $15.00 USD Received 15 Apr 2008; revised 14 Jul 2008; accepted 14 Jul 2008; published 18 Jul 2008

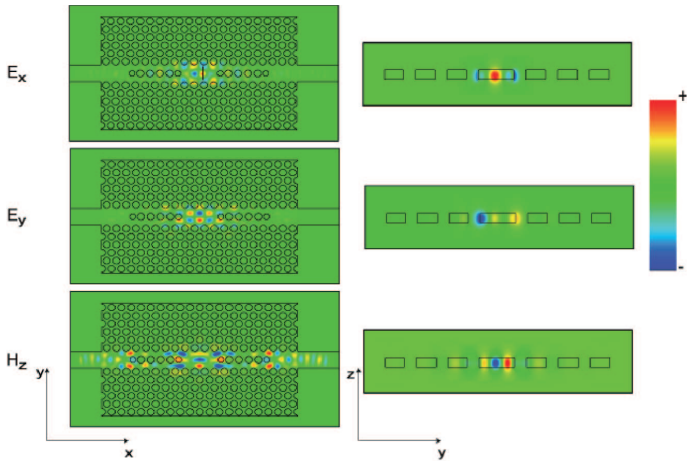

Fig. 6. (Color online) Spatial distribution of the electromagnetic field for the frequency corresponding to the transmission peak (see text).

to $n = 3.471$ as the pump is introduced). The red curve in Fig. 5 shows the transmission spectrum in a switching configuration. It can be noticed that the confined mode shifts its energy to higher frequency. In order to understand the physical origin of these transmission peaks appearing below the band edge we calculated the spatial distribution of the electromagnetic field using FDTD. For the peak of interest to us, that is the lowest energy one, the obtained results are presented in Fig. 6. As we can see, the electromagnetic field is strongly confined in the surroundings of the L3 cavity, evidencing a localized cavity mode. Therefore we have chosen this peak present in the experimental transmission spectra to carry out all optical switching. Notice that the confined field profile shown in Fig. 6 justifies the local refractive index modification in the cavity region used in Fig. 5. We expect a low pump pulse energy to be needed to switch the spectral position of this cavity mode as the electromagnetic field is strongly localized in the dielectric region, being the one subject to a change in the refractive index due to free carrier injection.

4.2. All optical switching

We next present the results regarding the all optical switching of the transmission through the samples containing L3 cavities. As mentioned above we will concentrate on the sample having 6-hole mirrors forming the cavity (i.e. sample A), being the one presenting a larger transmission at the cavity mode. Our choice for temporally modifying the optical response of the sample is to optically generate free carriers in the silicon matrix by pumping with a pulsed laser beam having a frequency above its band edge. Although this method can lead to an inhomogeneous excitation of free carriers in more bulky samples [8], for the present case dealing with thin slab PhC we have estimated a variation of less than 25% in the generated carrier density along the pump direction.

It is well known that optically injecting free carriers into a semiconductor produces a change in its dielectric function through a Drude contribution [25]:

$$\varepsilon(\omega) = \varepsilon_B(\omega) + \Delta\varepsilon_{eh}(\omega) = \varepsilon_B(\omega) - \left(\frac{\omega_p}{\omega}\right)^2 \frac{1}{1+\frac{i}{\omega\tau_D}}$$

being τ_D the Drude damping time. The carrier density enters the dielectric function variation

#95023 - $15.00 USD Received 15 Apr 2008; revised 14 Jul 2008; accepted 14 Jul 2008; published 18 Jul 2008

through the plasma frequency:

$$\omega_p = \sqrt{\frac{N_{eh}e^2}{\varepsilon_0 m_e m_{opt}}}$$

where e is the electronic charge, N_{eh} the free carrier density, m_e is the electron mass and m_{opt} is the optical effective mass of the carriers in units of the electron mass. If one assumes a density of generated free carriers $N_{eh} < 10^{22}$ cm^{-3} , it can be shown [26] that the change in refractive index of silicon is given by[1]:

$$n = n_0 - \frac{e^2}{2n_0\varepsilon_0 m_{opt} m_e \omega^2} N_{eh}$$

and hence one can reduce the refractive index of the silicon backbone, modifying the optical response of the PhC[2]. In our calculations, the numerical values for $m_{opt} = 0.15$ and $\tau_D = 10^{-13}$ s were taken from Ref. [26].

The pump beam is focussed to a circular spot with a 4 micron radius in order to modify the optical response of the sample only locally in the surroundings of the cavity, hence requiring a much lower energy than by illuminating the whole sample. In order to record the switching of the transmission spectrum, we temporally track the transmittance of the probe beam at a fixed wavelength (λ_p) in the time lapse of the pump pulse (2.5 ns). This operation is repeated for different values of λ_p in the surroundings of the center wavelength of the cavity mode (λ_c), and the set of transmission changes (ΔT) gives us the switched spectra.

Figure 7 shows the time evolution in the transmittance of the probe beam together with the pump intensity when the former is tuned to λ_c. For times shorter than the arrival of the pump pulse, no change is observed in the transmitted intensity. Small oscillations can be noticed in the transmitted signal, probably due to light interference and noise. As the pump pulse arrives, we see a dramatic drop in transmission as a consequence of the reduction in the refractive index of the silicon backbone taking place due to the injection of free carriers. The temporal width of the transmission drop equals that of the pump pulse (2.5 ns), indicating that all generated free carriers recombine in a timescale much smaller than the one we have access to with the current experimental setup. Recombination times, dictating the speed of the switching process are strongly affected by the microstructure of the silicon backbone. The longest time limit is that dictated by the bulk value of silicon, but much shorter times can take place due to surface recombination or the presence of defects, which can yield recovery times of tens of ps as recently reported [15, 17]. It remains a task for the future to study the time scales of signal recovery in our system.

Prior to perform the switching of the transmission peak we verified that the observed peak corresponds indeed to a mode localized within the cavity. To do so we tried pumping at different sample locations including several points along the W1.5 waveguide and points in the 2D crystal. We found that only when the pump beam is centered at the cavity, the transmission experiences a change with the injection of free carriers. This proves that the origin of the change in transmission is switching of a localized cavity mode.

In order to obtain the switched transmission spectrum, we have repeated the above procedure for different λ_p in the surroundings of λ_c. Figure 8 shows some of the results obtained for certain representative wavelengths. When λ_p is smaller than λ_c, we obtain a positive change in

[1]In estimating the density of free carriers generated N_{eh} we have taken into account a factor f=0.6 which accounts for the losses of the pump beam due to reflectance at the sample surface.

[2]We have discarded refractive index variations associated with temperature changes originating at non radiative electron-hole recombination processes in the silicon matrix. The fastest reported rise time for these processes is 100 ns (see Ref. [4]) and hence much slower than our pump pulses. Also, the repetition rate employed in our set-up allows heat diffusion without rising the system temperature.

#95023 - $15.00 USD Received 15 Apr 2008; revised 14 Jul 2008; accepted 14 Jul 2008; published 18 Jul 2008

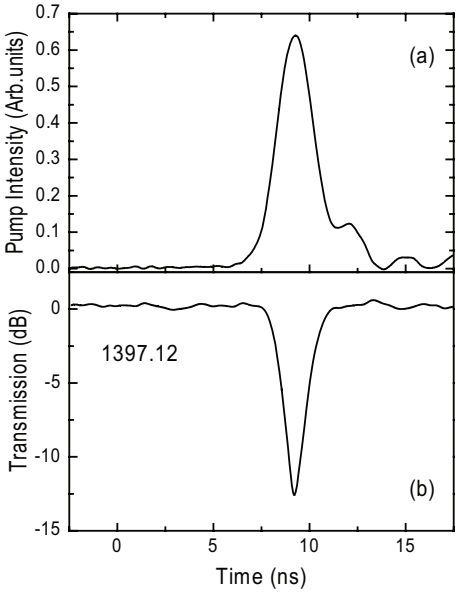

Fig. 7. (a) Time evolution of the 532 nm pump pulse employed to inject free carriers into the sample. (b) Change in transmission through the sample at a wavelength λ_c in the same time scale as for the pump pulse.

transmission ($\Delta T > 0$) as a result of the blueshift of the cavity mode as expected when reducing the refractive index of the silicon backbone by injecting free carriers (Fig. 8(a) and 8(b)). If the probe wavelength gets sufficiently close to λ_c but still remaining smaller the response in time is more complex and quite interesting (Fig. 8(c)). As the pump pulse shifts the resonance, ΔT is first positive until the resonance maximum reaches the probe wavelength, then the ΔT becomes negative as λ_p falls on the right shoulder of the resonance. When the intensity of the pulse decreases, the system starts to recover the initial state and the reverse behavior occurs with another maximum of ΔT, then the transmission decreases again. Notice that the temporal behavior of ΔT is not symmetric, due to the asymmetry of the laser pulse as shown in Fig. 7(a). Finally, when $\lambda_p \geq \lambda_c$ we observe a negative change $\Delta T < 0$ (Fig.s 8(d)–8(f)) which achieves a maximum when $\lambda_p = \lambda_c$. We can see how to achieve both, an OFF/ON (Fig.s 8(b)) or ON/OFF (Fig.s 8(e)) scenario by placing the probe wavelength at the appropriate side of the cavity mode. We can notice that the switching signal is almost the same for the two configurations.

Figure 9 shows the reconstruction of the switched spectra done by collecting the ΔT's obtained as mentioned above. We can see how the resonance peak is shifted by 0.37 nm, its full width at half maximum (FWHM), in this way achieving a modulation of the transmitted intensity of 90%. The minimum power needed to switch the transmitted signal, that is to shift the resonance peak by its FWHM, is of 140 nW in our case. This corresponds to a pulse energy of 13 pJ which, when focussed to a 4 micron spot, yields an intensity at the sample surface of 11 KW/cm^2. According to the expressions presented above, with such an intensity we can excite a free carrier density of $N_{eh} = 5.4 \cdot 10^{18}$ cm^{-3} which correspond to a refractive index change of 0.22% with respect to the bulk value of silicon [27]. The pulse energy employed for switching the resonance peak is comparable to the lowest energies obtained in a similar configuration, namely shifting a resonant state by free carrier injection generated by linear absorption [11] and only slightly higher than in Ref. [12] where both probe and pump beams propagate in the

#95023 - $15.00 USD Received 15 Apr 2008; revised 14 Jul 2008; accepted 14 Jul 2008; published 18 Jul 2008

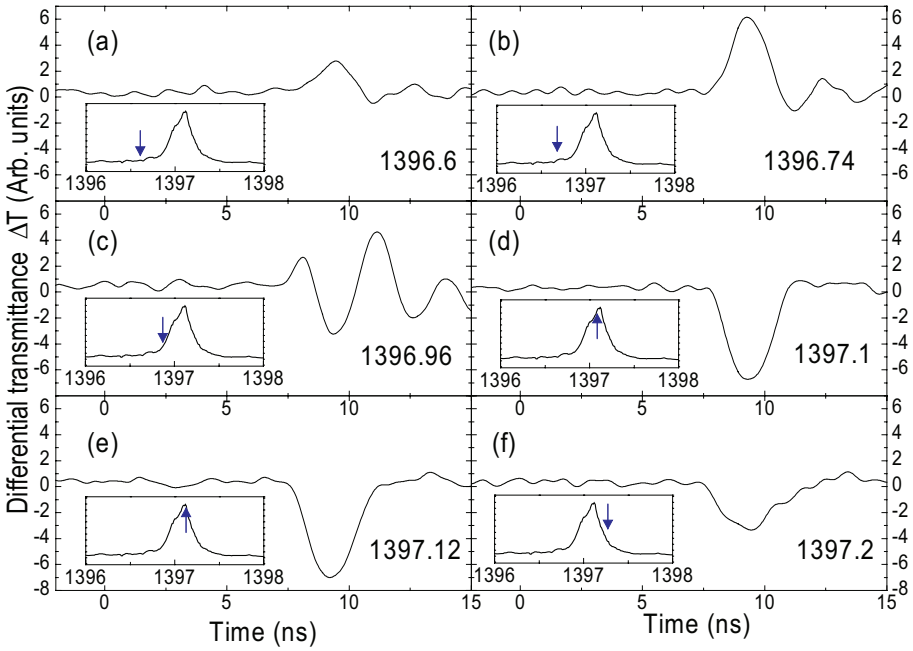

Fig. 8. Change in transmission of the probe beam in the time lapse when the system is optically pumped. (a)-(f) Show the evolution for different probe wavelengths (λ_p) in the surroundings of the cavity mode center (λ_c). The inset shows the position of the probe wavelength indicated with the blue arrows to respect the resonance.

waveguide and two–photon absorption is employed. Finally, we have estimated the absorption induced in the probe beam by the generation of the free carrier plasma, employing the above expressions for the refractive index change. From the imaginary contribution to the refractive index ($5 \cdot 10^{-5}$) we have obtained a linear absorption coefficient of about 2 mm^{-1}, which is negligible compared to other sources of losses typically present in PhC slab waveguides such as roughness scattering [28].

#95023 - $15.00 USD Received 15 Apr 2008; revised 14 Jul 2008; accepted 14 Jul 2008; published 18 Jul 2008

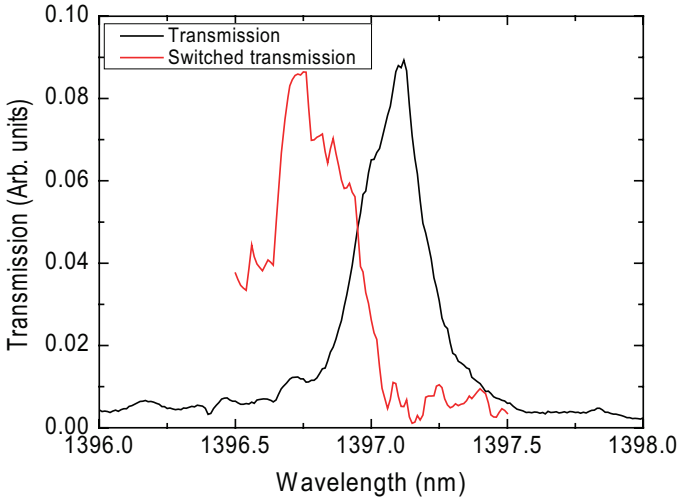

Fig. 9. (Color online) Transmission spectrum of the cavity mode in the linear regime (black line) and under optical pumping (red line).

5. Conclusions

We have fabricated and optically characterized 2D PhCs containing W1.5 waveguides coupled with L3 cavities on silicon membranes. By means of optically generated free carriers, all-optical switching has been demonstrated at the spectral position of a localized cavity mode. Employing low energy (pJ) pulses, modulation amplitudes of 90% have been demonstrated in a nanosecond scale with negligible absorption. The present W1.5 waveguides, with increased channel width and low propagation losses, have been demonstrated to be suitable for introducing cavity structures performing all-optical switching functions.

Acknowledgments

J.F. Galisteo-López was sponsored by the Postdoctoral Program of the Spanish Ministry of Science and Education. This work was supported by Fondazione CARIPLO and by Italian Ministry of University and research through FIRB contract #RBAP06L4S5.

#95023 - $15.00 USD Received 15 Apr 2008; revised 14 Jul 2008; accepted 14 Jul 2008; published 18 Jul 2008